Electronic Supplementary Material (ESI) for Journal of Materials Chemistry A.

Synergistically toughening nacre-like graphene nanocomposites *via* gel-film transformation

Shanshan Gong,[a†] Qi Zhang,[a†] Ruliang Wang,[b†] Lei Jiang[a] and Qunfeng Cheng[a*]

[a]Key Laboratory of Bio-inspired Smart Interfacial Science and Technology of Ministry of Education, School of Chemistry, Beijing Advanced Innovation Center for Biomedical Engineering, Beihang University

Beijing 100191, P. R. China

E-mail: cheng@buaa.edu.cn

[b]Department of Breast Cancer, the Affiliated Hospital of Academy of Military Medical Sciences, Beijing, 100071, P. R. China

[†]These three authors contribute equally to this work.

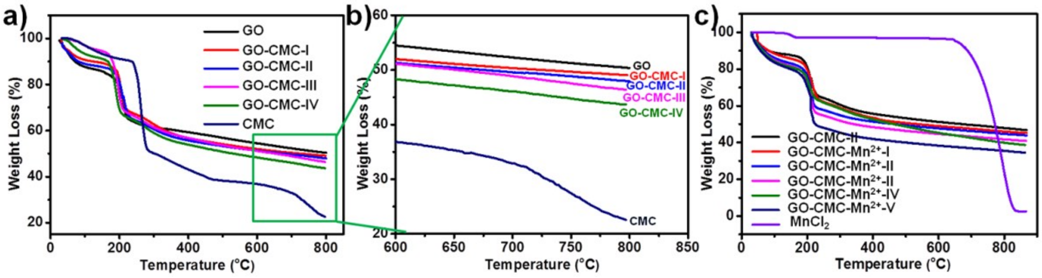

Figure S1. a) and b) TGA curves of pure GO and CMC films, and GO-CMC hybrid layered materials with different CMC contents. c) TGA curves of $MnCl_2$ power, GO-CMC-II and GO-CMC-Mn^{2+} composite films with different Mn^{2+} contents. The curves were obtained under the atmosphere of nitrogen with a temperature rising rate of 10°C·min^{-1}.

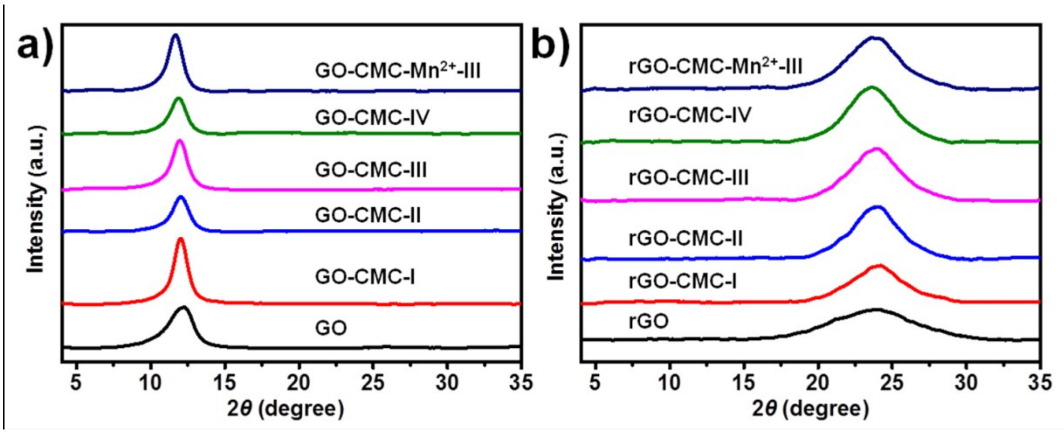

Figure S2. XRD spectrum of pure GO film, GO-CMC and GO-CMC-Mn^{2+}-III composite films (a) before and (b) after chemical reduction, respectively. The *d*-spacing of the nanocomposites rises with the increasing of CMC polymer and the introducing of Mn^{2+}.

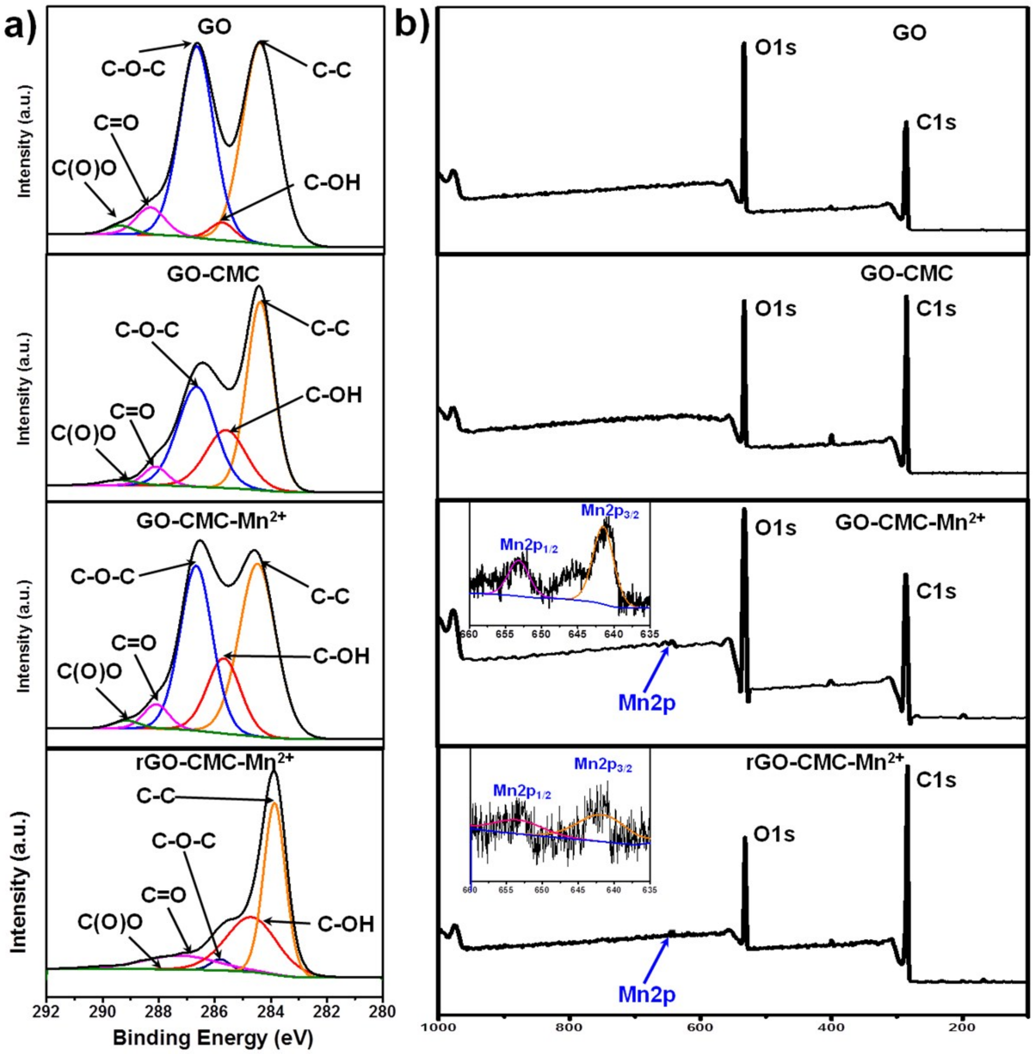

Figure S3. (a) C1s XPS survey spectra of pure GO film, GO-CMC, GO-CMC-Mn^{2+} and rGO-CMC-Mn^{2+} nanocomposites and (b) the corresponding whole spectrum.

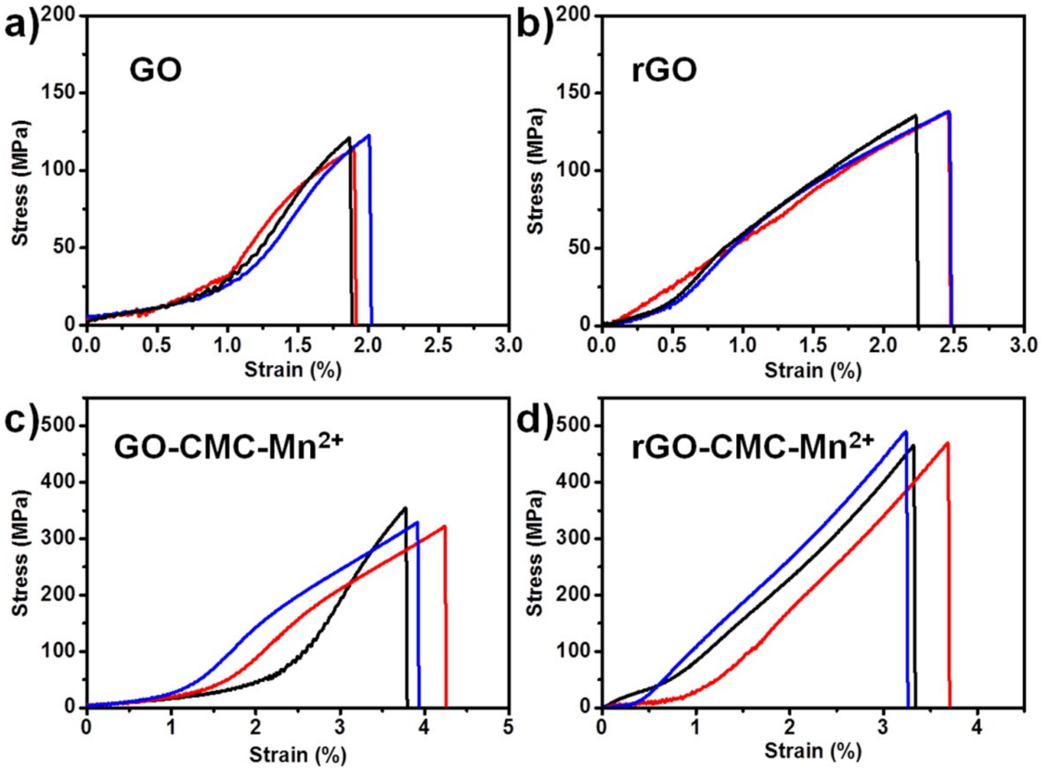

Figure S4. The stress-strain curves of pure GO film, rGO film, GO-CMC-Mn^{2+} nanocomposites, and rGO-CMC-Mn^{2+} bioinspired nanocomposites, demonstrating the resultant rGO-CMC-Mn^{2+} nanocomposites have excellent mechanical properties, superior to GO, rGO and GO-CMC-Mn^{2+} materials.

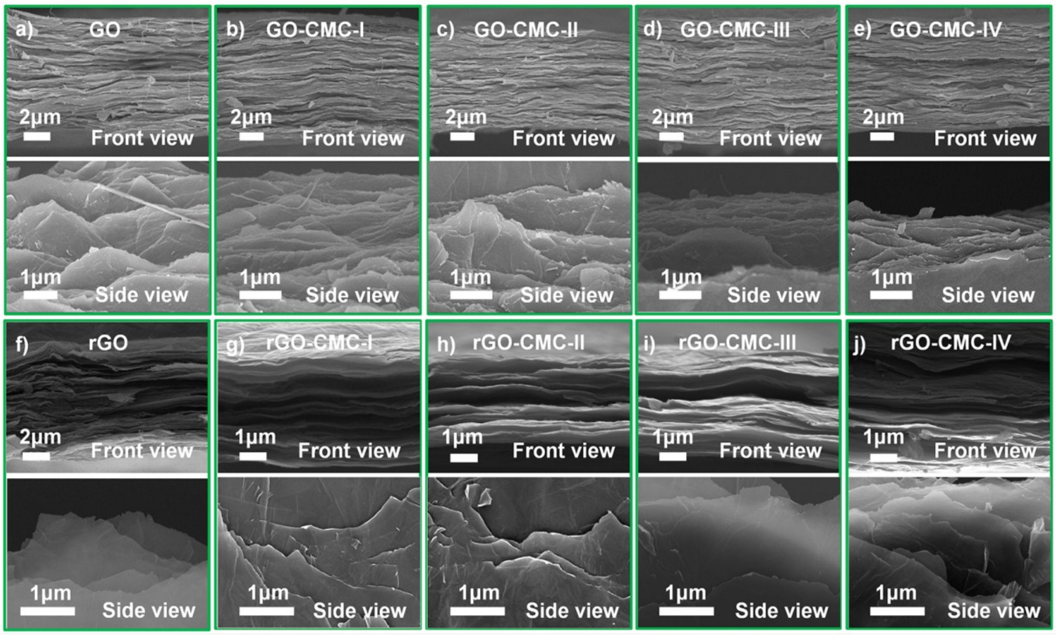

Figure S5. The front and side view fracture morphologies of pure GO film and GO-CMC nanocomposites, respectively. a) GO film, b) GO-CMC-I, c) GO-CMC-II, d) GO-CMC-III, e) GO-CMC-IV, f) rGO, g) rGO-CMC-I, h) rGO-CMC-II, i) rGO-CMC-III, and j) rGO-CMC-IV nanocomposites, respectively.

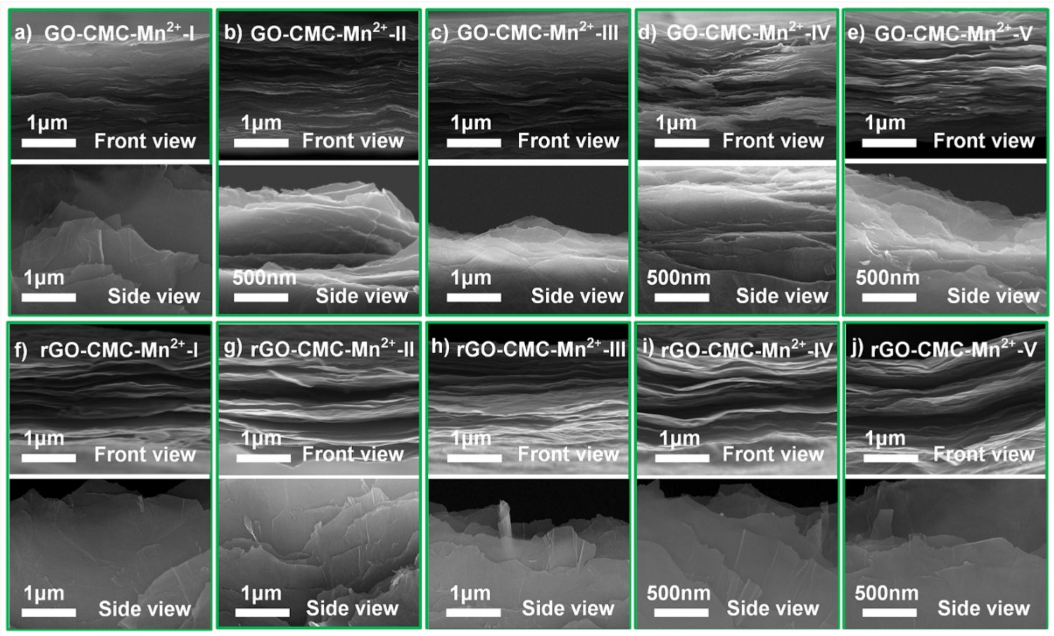

Figure S6. The front and side view fracture morphologies of GO-CMC-Mn^{2+} nanocomposites with different concentrations of Mn^{2+}. a) GO-CMC-Mn^{2+}-**I**, b) GO-CMC-Mn^{2+}-**II**, c) GO-CMC-Mn^{2+}-**III**, d) GO-CMC-Mn^{2+}-IV, e) GO-CMC-Mn^{2+}-V, f) rGO-CMC-Mn^{2+}-**I**, g) rGO-CMC-Mn^{2+}-**II**, h) rGO-CMC-Mn^{2+}-**III**, i) rGO-CMC-Mn^{2+}-IV, and j) rGO-CMC-Mn^{2+}-V nanocomposites, respectively.

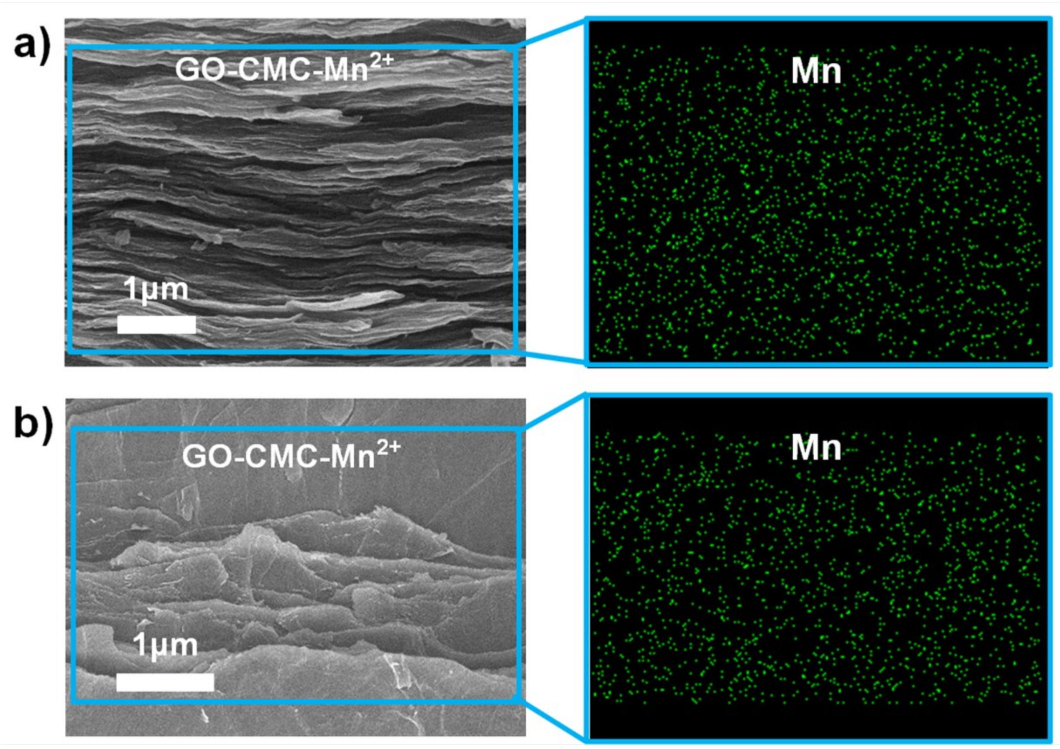

Figure S7. a) The cross-section morphology and EDS of the GO-CMC-Mn^{2+} nanocomposites. b) The vertical view morphology and EDS of the GO-CMC-Mn^{2+} nanocomposites. The EDS results indicate the uniform distribution of Mn element in the GO-CMC-Mn^{2+} nanocomposites.

Table S1. The exact GO content of GO-CMC nanocomposite films determined by TGA under nitrogen atmosphere with a temperature rising rate of 10 ºC/min.

Sample	Input GO Content (wt%)	GO content by TGA (wt%)
GO	100	/
GO-CMC-I	95	95.3
GO-CMC-II	90	91.3
GO-CMC-III	85	85.8
GO-CMC-IV	80	79.5

Table S2. The exact Mn^{2+} content of GO-CMC-Mn^{2+} nanocomposite films determined by TGA under nitrogen atmosphere with a temperature rising rate of 10 ºC/min.

Sample	Mn^{2+} content by TGA (wt%)	GO-CMCcontent by TGA (wt%)
GO-CMC-II	/	100
GO-CMC-Mn^{2+}-I	1.54	96.47
GO-CMC-Mn^{2+}-II	2.81	93.56
GO-CMC-Mn^{2+}-III	5.75	86.82
GO-CMC-Mn^{2+}-IV	7.96	81.77
GO-CMC-Mn^{2+}-V	12.01	72.48

Table S3. The d-spacing of pure GO film, GO-CMC and GO-CMC-Mn^{2+} nanocomposites before and after HI reduction.

Sample	*2θ*	d（Å）
GO	12.24	7.23
GO-CMC-I	12.02	7.36
GO-CMC-II	12.00	7.37
GO-CMC-III	11.98	7.39
GO-CMC-IV	11.90	7.43
GO-CMC-Mn^{2+}-III	11.68	7.57
rGO	24.08	3.69
rGO-CMC-I	24.14	3.69
rGO-CMC-II	24.02	3.70
rGO-CMC-III	23.88	3.73
rGO-CMC-IV	23.64	3.76
rGO-CMC-Mn^{2+}-III	23.58	3.77

Table S4. The mechanical properties of pure GO film, pure CMC, GO-CMC and GO-CMC-Mn^{2+} materials.

Sample	Before HI reduction		After HI reduction	
	Tensile strength (MPa)	Toughness (MJ/m^3)	Tensile strength (MPa)	Toughness (MJ/m^3)
GO	118.9 ± 4.8	0.9 ± 0.1	140.8 ± 4.7	1.6 ± 0.1
CMC	114.9 ± 2.8	11.5 ± 0.4	/	/
GO-CMC-I	228.6 ± 4.4	3.5 ± 0.5	295.7 ± 2.4	4.2 ± 0.4
GO-CMC-II	274.1 ± 7.6	3.64 ± 0.3	372.7 ± 7.3	5.2 ± 0.4
GO-CMC-III	194.3 ± 2.1	2.5 ± 0.3	292.2 ± 11.6	3.9 ± 0.4
GO-CMC-IV	185.4 ± 7.0	2.3 ± 0.2	238.4 ± 19.5	3.1 ± 0.7
GO-CMC-Mn-I	262.8 ± 10.4	2.6 ± 0.4	351.4 ± 2.5	4.1 ± 0.2
GO-CMC-Mn-II	275.1 ± 11.3	2.7 ± 0.5	376.2 ± 9.0	4.6 ± 0.7
GO-CMC-Mn-III	329.2 ± 5.7	5.5 ± 0.2	475.2 ± 13.0	6.6 ± 0.3
GO-CMC-Mn-IV	280.3 ± 2.7	4.2 ± 0.1	337.9 ± 3.5	4.2 ± 0.1
GO-CMC-Mn-V	274.8 ± 4.6	4.2 ± 0.6	330.3 ± 13.6	3.6 ± 0.3

Table S5. The mechanical properties of the natural nacre and other GO-based nanocomposites.

Materials	Synthesis strategy	Tensile strength (MPa)	Toughnes s (MJ/m^3)	Reference
Nacre		200	2.6	2
GO-PMMA	vacuum-assisted self-assembly	148.3	2.35	7
rGO-PVA	solution-casting	188.9	2.52	8
rGO-SF	filtration	300	2.8	38
GO-SF	layer-by-layer	292.4	3.42	37
GO-Ca^{2+}	filtration	125.8	0.31	34
GO-Mg^{2+}	filtration	80.6	0.13	34
rGO-Cu^{2+}	--	335	0.5	32
GO-Al^{3+}	vacuum	100.5	0.23	39
GO-Fe^{3+}-TA	vacuum	169.27	0.42	23
GO-PI–Mg^{2+}	evaporation	90.6	5.04	40
GO-PVP	gel-film transformation	209	2.84	11
GO-$G4NH_2$	gel-film transformation	253	5.75	11
GO-PVA	gel-film transformation	236	3.95	11
GO-CMC	gel-film transformation	234	4.45	11
GO-PEI	gel-film transformation	253	5.51	11
GO-PEO	gel-film transformation	236	5.02	11
rGO-CS	gel-film transformation	424	8.98	11
GO-SF	solution casting	221	2.0	36
rGO-PAPB	gel-film transformation	382	7.50	10
rGO-CMC-	gel-film transformation	475.2	6.6	This work

Mn^{2+}

Table S6. The electrical properties of pure rGO film, rGO-CMC and rGO-CMC-Mn^{2+} nanocomposites.

sample	Electrical conductivity (S/cm)
rGO	315.0 ± 12.9
rGO-CMC-I	313.5 ± 6.5
rGO-CMC-II	311.6 ± 4.4
rGO-CMC-III	296.9 ± 13.0
rGO-CMC-IV	254.9 ± 10.9
rGO-CMC-Mn^{2+}-I	297.1 ± 5.0
rGO-CMC-Mn^{2+}-II	276.1 ± 16.2
rGO-CMC-Mn^{2+}-III	268.2 ± 11.4
rGO-CMC-Mn^{2+}-IV	266.7 ± 14.1
rGO-CMC-Mn^{2+}-V	182.6 ± 10.9